# ARTICLE

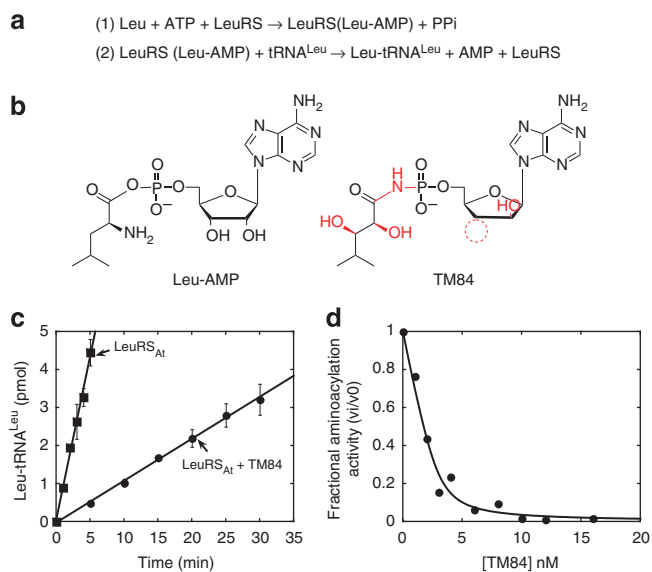# Plant tumour biocontrol agent employs a tRNA-dependent mechanism to inhibit leucyl-tRNA synthetase

Shaileja Chopra[1,*], Andrés Palencia[2,*], Cornelia Virus[1], Ashutosh Tripathy[3], Brenda R. Temple[4], Adrian Velazquez-Campoy[5], Stephen Cusack[2] & John S. Reader[1]

Leucyl-tRNA synthetases (LeuRSs) have an essential role in translation and are promising targets for antibiotic development. Agrocin 84 is a LeuRS inhibitor produced by the biocontrol agent *Agrobacterium radiobacter* K84 that targets pathogenic strains of *A. tumefaciens*, the causative agent of plant tumours. Agrocin 84 acts as a molecular Trojan horse and is processed inside the pathogen into a toxic moiety (TM84). Here we show using crystal structure, thermodynamic and kinetic analyses, that this natural antibiotic employs a unique and previously undescribed mechanism to inhibit LeuRS. TM84 requires tRNA[Leu] for tight binding to the LeuRS synthetic active site, unlike any previously reported inhibitors. TM84 traps the enzyme–tRNA complex in a novel 'aminoacylation-like' conformation, forming novel interactions with the KMSKS loop and the tRNA 3'-end. Our findings reveal an intriguing tRNA-dependent inhibition mechanism that may confer a distinct evolutionary advantage *in vivo* and inform future rational antibiotic design.

---

[1] Department of Cell Biology and Physiology, The University of North Carolina at Chapel Hill, 536 Taylor Hall, CB# 7090, Chapel Hill, North Carolina 27599-7090, USA. [2] European Molecular Biology Laboratory, Grenoble Outstation and Unit of Virus Host-Cell Interactions, UJF-EMBL-CNRS, UMI 3265, 6 rue Jules Horowitz, BP181, 38042 Grenoble Cedex 9, France. [3] UNC Macromolecular Interactions Facility, The University of North Carolina at Chapel Hill, 1124 Genome Sciences Building, CB# 3280, 250 Bell Tower Drive, Chapel Hill, North Carolina 27599-3280, USA. [4] R. L. Juliano Structural Bioinformatics Core Facility, The University of North Carolina at Chapel Hill, Chapel Hill, North Carolina 27599, USA. [5] Institute of Biocomputation and Physics of Complex Systems (BIFI), Universidad de Zaragoza, 50018 Zaragoza; Unidad Asociada BIFI-IQFR-CSIC; and Fundacion ARAID, Government of Aragon, Spain. * These authors contributed equally to the work. Correspondence and requests for materials should be addressed to J.S.R. (email: jreader@med.unc.edu).

Leucyl-tRNA synthetases (LeuRSs) have an essential role in translating the genetic code by ligating leucine (Leu) to the 3′-end of tRNA$^{Leu}$. The LeuRS aminoacylation reaction is catalysed by a highly conserved catalytic domain encoding a nucleotide-binding Rossman fold, and the class I aminoacyl-tRNA synthetase (aaRS)-defining catalytic peptide sequences, the HIGH and KMSKS motifs[1,2]. The reaction is catalysed in a two-step mechanism (Fig. 1a): in the tRNA-independent first step, Leu is activated by ATP to form a tightly-bound high-energy intermediate Leu-AMP and release of inorganic pyrophosphate; in the second step, Leu-AMP reacts with the 2′-hydroxyl (-OH) of the terminal ribose at the 3′-end of the tRNA$^{Leu}$ to form Leu-tRNA$^{Leu}$ (ref. 3). LeuRSs are also composed of a number of additional domains involved in binding tRNA$^{Leu}$ or in proofreading activities[4–7]. X-ray crystal structures have been obtained for LeuRSs from both archaeal and bacterial origins in complex with a number of substrates and substrate analogues, including Leu[5] and tRNA$^{Leu}$ (refs 6,7), a reaction-intermediate analogue of Leu-AMP[5], and also substrate mimics of both post- and pre-transfer editing reactions[8]. The range of different LeuRS conformations visualized by these studies highlights the complex interplay of these multi-domain enzymes with their substrates.

LeuRSs, and the other aaRSs, are essential enzymes that are underutilized targets for the development of antibiotics[9]. The most prominent inhibitor class that has been investigated are the rationally designed stable analogues of aminoacyl-adenylates (AA-AMPs)[10–12], such as leucyl-adenylate sulphamoyl analogue (Leu-AMS), which was used in X-ray crystallographic studies of LeuRS to define the binding pocket of the reaction intermediate[5]. Stable AA-AMP analogues have proven to be potent inhibitors of a range of other aaRSs[13,14]. They are thought to act by competing with the amino-acid and ATP substrates for binding to the synthetic active site contained in the catalytic domain, thereby inhibiting the amino-acid activation reaction and consequently aminoacylation.

Agrocin 84 is a recently identified inhibitor of LeuRS[15,16]. The antibiotic is produced by the biocontrol agent *Agrobacterium radiobacter* strain K84 that is used worldwide to protect plants against the economically important disease crown gall[17]. The bacterial pathogen *A. tumefaciens* is the causative agent of the disease and induces tumours into infected plants via the transfer of oncogenic DNA[18]. Agrocin 84 specifically targets strains of *A. tumefaciens* by acting as a molecular Trojan horse that mimics a plant tumour-derived substrate to gain access into the agrobacterial cell[19,20]. Once inside, agrocin 84 is processed into a toxin, TM84, which we have shown to be a potent inhibitor of the *A. tumefaciens* genome-encoded LeuRS (LeuRS$_{At}$)[16]. TM84 closely resembles the obligate reaction intermediate of LeuRSs, Leu-AMP (Fig. 1b), but contains a relatively stable *N*-acyl 5′-phosphoramidate bond instead of the labile phosphoanhydride linkage.

We previously hypothesized that TM84 acts as a stable analogue of Leu-AMP and inhibits LeuRS by binding to the synthetic active site[16]. Surprisingly, we now show that TM84 is different from Leu-AMP analogues, as it employs a unique tRNA-dependent inhibition mechanism in which the 3′-end of tRNA$^{Leu}$ is required to form an 'aminoacylation-like' conformation that stabilizes the binding of the inhibitor in a ternary inhibition complex. Our structure, together with a recently published structure of an *Escherichia coli* LeuRS · tRNA$^{Leu}$ · Leu-AMP analogue[21], reveal exciting new insights into the recognition of tRNA$^{Leu}$ by LeuRS during aminoacyl transfer, and molecular details of how the enzyme catalyses the second stage of the aminoacylation reaction.

## Results

**TM84 is a tight-binding inhibitor of tRNA$^{Leu}$ aminoacylation.** To determine the mechanism by which TM84 inhibits LeuRS$_{At}$, we examined inhibition of the leucylation reaction using an *in vitro* transcribed substrate encoding the tRNA$^{Leu}$(UAA) *A. tumefaciens* isoacceptor. Our results clearly show substantial inhibition of the aminoacylation reaction at concentrations of TM84 ([I] = 3 nM) similar to that of the LeuRS$_{At}$ enzyme ([E] = 4 nM) (Fig. 1c). The stoichiometric levels of TM84 to enzyme required to see inhibition strongly suggested that TM84 is a tight-binding inhibitor of LeuRS$_{At}$, and therefore required the use of non-Michaelis–Menten kinetic analysis of subsequent inhibition assays to determine the true potency of the inhibitor[22].

Tight-binding inhibitors often display a slow onset of inhibition due to conformational changes of the enzyme on inhibitor binding[23]. This behaviour is typically manifested as a curvilinear appearance to enzyme initial rates that cannot be adequately analysed using the standard discontinuous assays used for aaRSs. To eliminate the potential complexity of slow binding effects on our analysis, TM84 was pre-incubated with the enzyme and tRNA$^{Leu}$ before initiating the aminoacylation reaction. We then plotted the fraction of the aminoacylation rate measured against [TM84] and fit the resulting dose–response curve (Fig. 1d) to the Morrison equation for tight-binding inhibitors. The fit showed an apparent $K_i$ ($K_i^{app}$) of $0.3 \pm 0.1$ nM, which suggests that TM84 behaves as a tight-binding inhibitor of LeuRS$_{At}$ (ref. 22).

**TM84 weakly inhibits Leu-AMP formation in the absence of tRNA$^{Leu}$.** We previously hypothesized that TM84 competes with Leu and ATP for binding to the synthetic active site[16]. To test this, we examined if TM84 could inhibit activation of Leu by ATP in a similar manner to Leu-AMS. We made use of the ATP/pyrophosphate exchange reaction (ATP/PPi), which measures the rate of Leu-AMP formation by the enzyme, in the presence of Leu

### a

(1) Leu + ATP + LeuRS → LeuRS(Leu-AMP) + PPi

(2) LeuRS (Leu-AMP) + tRNA$^{Leu}$ → Leu-tRNA$^{Leu}$ + AMP + LeuRS

### b



### c



### d



**Figure 1 | TM84 is a tight-binding inhibitor of the LeuRS$_{At}$ aminoacylation reaction.** (**a**) Aminoacylation reaction of LeuRS. (**b**) Comparison of Leu-AMP and TM84—differences in red. (**c**) Inhibition of LeuRS$_{At}$ (4 nM) aminoacylation reaction +/− TM84 (3 nM). Error bars on the initial rate time points represent standard deviation, $n = 3$. (**d**) The TM84 dose–response curve of LeuRS$_{At}$ (4 nM) aminoacylation reaction was fit to the Morrison equation for tight-binding inhibitors (equation (1)), indicating a $K_{i\ app}$ of $0.3 \pm 0.1$ nM.

and ATP substrates, through addition of excess [$^{32}$P]-labelled inorganic PPi that leads to formation of [$\gamma$-$^{32}$P] ATP via a back reaction[24,25]. Thus, it is possible to observe the enzyme catalysing multiple turnovers of the Leu activation reaction. As expected, our results show that Leu-AMS is a potent inhibitor of the LeuRS$_{At}$-catalysed ATP/PPi exchange reaction (Supplementary Fig. S1). Surprisingly, TM84 did not potently inhibit amino-acid activation (Fig. 2a). High concentrations of TM84 (limited by availability of this natural product) were required to see even partial inhibition (Fig. 2b).

A potential explanation of how TM84 can be a strong inhibitor of the overall aminoacylation, yet not the Leu activation reaction, could be a requirement for tRNA$^{Leu}$ in the inhibition mechanism. To test this, we examined if TM84 inhibition of the LeuRS$_{At}$ aminoacylation activity could be reduced using low concentrations of tRNA$^{Leu}$ substrate. However, the low concentrations of tRNA required to see activity in these assays made quantitation of Leu-tRNA$^{Leu}$ difficult, even when sensitive TLC-based assays were used. To circumvent this, we explored the requirement for tRNA$^{Leu}$ in the inhibition mechanism of TM84 by adding *in vitro* transcribed tRNA$^{Leu}$ to the ATP/PPi-exchange reaction. This approach has been used before for aaRS enzymes such as glutaminyl-[26] and glutamyl-tRNA synthetases[27], which, unlike LeuRSs, require tRNA for the activation reaction to proceed. Importantly, in these experiments we used an active tRNA$^{Leu}$ concentration of 6.7 $\mu$M that had no effect on the initial rate of ATP/PPi exchange for the LeuRS$_{At}$ reaction (Fig. 2a). In addition, negligible amounts of Leu-tRNA$^{Leu}$, the product of the aminoacylation reaction, were detectable under these reaction conditions ([LeuRS$_{At}$] = 1 nM (Supplementary Fig. S2)). Our experiments were performed $+/-$ tRNA$^{Leu}$ and by varying the [TM84]. The resulting dose–response data were analysed as detailed previously[28] and showed a greater than 4 orders of magnitude increase in the inhibition of the amino-acid activation reaction with tRNA$^{Leu}$ compared to that without tRNA$^{Leu}$ (IC$_{50}$ $_{TM84}$ = >25 $\mu$M and IC$_{50}$ $_{TM84 \cdot tRNA}$ = 0.7 $\pm$ 0.1 nM; see Fig. 2b). These results were strongly suggestive that tRNA$^{Leu}$ actively participates in the inhibition mechanism of TM84 for LeuRS$_{At}$, but also did not rule out that TM84 binds to an alternative site on the enzyme.

Some tight-binding enzyme inhibitors form covalent bonds with protein residues (or RNA substrates), leading to irreversible interactions[22,29]. To determine if this was the case with the interaction of TM84 with LeuRS$_{At}$, we pre-incubated LeuRS$_{At}$ with TM84 and tRNA$^{Leu}$ and then added an RNase cocktail to degrade the tRNA into mononucleotides. We then tested samples that had both been incubated $+/-$ RNase for activity in the ATP/PPi exchange experiment. The presence of tRNA potently inhibited the LeuRS$_{At}$ Leu activation reaction, whereas RNAse treatment completely restored activity in the presence of TM84 (Fig. 2c). This experiment demonstrates that TM84 binds reversibly to LeuRS$_{At}$ and also supports the idea that tRNA is essential for the tight binding of TM84 to LeuRS$_{At}$.

**tRNA$^{Leu}$ increases the binding affinity of TM84 for LeuRS$_{At}$.** To gain further insights into the unusual ternary inhibitor interaction, we employed isothermal calorimetry (ITC) to test the effect of tRNA$^{Leu}$ on the energetics of TM84 binding to LeuRS$_{At}$. Initially, we examined the two separate binding reactions of TM84 (Fig. 3a) and tRNA$^{Leu}$ to LeuRS$_{At}$ (Table 1). The two isotherms obtained for binding of TM84 to LeuRS$_{At}$ and tRNA$^{Leu}$ to LeuRS$_{At}$ both fit to single-site binding models with stoichiometries close to 1, and with a calculated $K_{d\ TM84}$ of 152 $\pm$ 20 nM and a $K_{d\ tRNA}$ of 84.9 $\pm$ 6.1 nM. We then examined the ternary equilibria after pre-incubation with tRNA$^{Leu}$ (Fig. 3a,b). For these
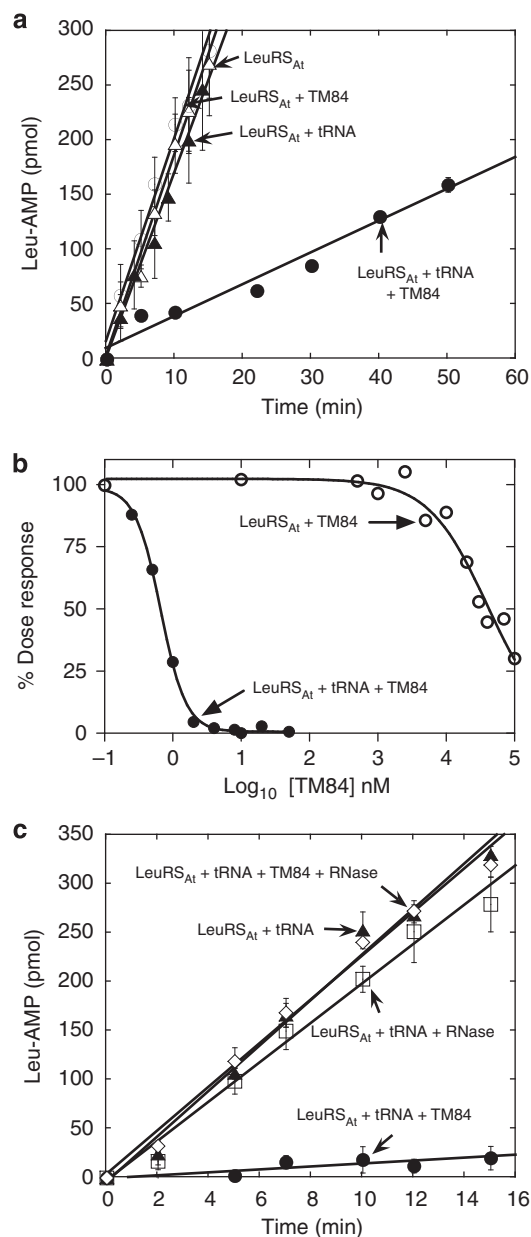


**Figure 2 | tRNA$^{Leu}$ is required for reversible TM84 inhibition of leucine activation.** (**a**) TM84 inhibition of LeuRS$_{At}$ (1 nM) ATP/PPi exchange reaction $+/-$ tRNA$^{Leu}$ (6.7 $\mu$M). Initial rate reaction conditions are LeuRS$_{At}$ only ($\triangle$), LeuRS$_{At}$ with 1 $\mu$M TM84 ($\bigcirc$), LeuRS$_{At}$ with tRNA$^{Leu}$ ($\blacktriangle$), and LeuRS$_{At}$ with tRNA$^{Leu}$ and 50 nM TM84 ($\bullet$). Error bars indicate standard deviation, n = 3. (**b**) TM84 dose–response curves of LeuRS$_{At}$-catalysed ATP/PPi-exchange reaction in the absence ($\bigcirc$) and presence ($\bullet$) of tRNA$^{Leu}$. IC$_{50}$ $_{TM84}$ > 25 $\mu$M and IC$_{50}$ $_{TM84 \cdot tRNA}$ < 1 nM. (**c**) Effect of RNase treatment on LeuRS$_{At}$·tRNA$^{Leu}$·TM84 complex ATP/PPi exchange activity. Reaction conditions examined were LeuRS$_{At}$ with tRNA$^{Leu}$ ($\blacktriangle$), LeuRS$_{At}$ with tRNA$^{Leu}$ and 250 nM TM84 ($\bullet$), preformed LeuRS$_{At}$·tRNA$^{Leu}$ complex treated with RNase ($\square$), and preformed LeuRS$_{At}$·tRNA$^{Leu}$·TM84 complex treated with RNase ($\diamondsuit$).

experiments, tRNA was first pre-bound to the protein in the ratio of 1.2:1. TM84 was then titrated into the protein–tRNA mixture to obtain the LeuRS·tRNA$^{Leu}$·TM84 complex. Surprisingly, the isotherms of the ternary equilibrium exhibited distinct biphasic forms that could not be fitted to a simple single-site model. Instead, the data could be successfully fitted to an independent
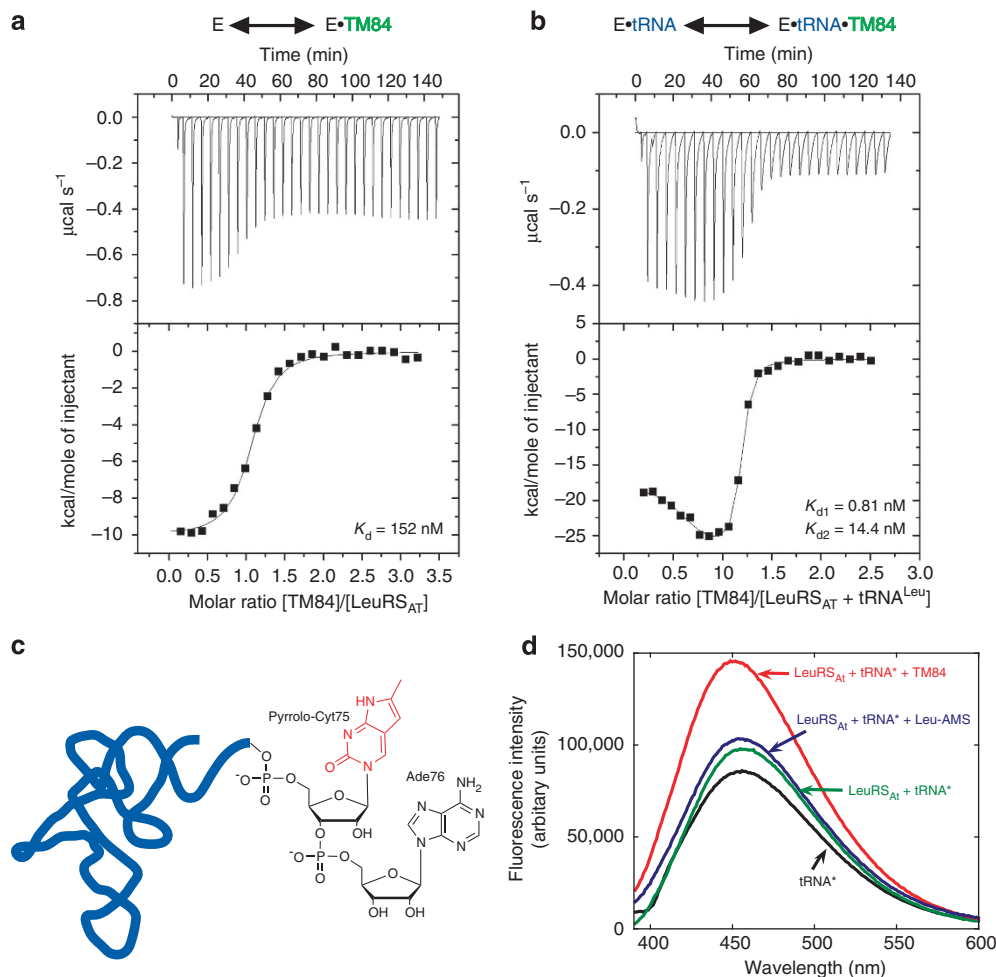
**Figure 3 | tRNA induces TM84 tight-binding and adopts the modified conformation. (a)** ITC titration of TM84 into LeuRS$_{At}$. The top panel shows raw thermogram and bottom panel shows the binding isotherm fitted to a single-site model (see Table 1 for thermodynamic values). **(b)** Titration of TM84 into LeuRS$_{At}$ · tRNA$^{Leu}$ complex. Bottom panel isotherm fitted to a two-independent-sites model. **(c)** Fluorescent tRNApyr$^{Leu}$ probe sensitive to the environment of the CCA 3′-end. Pyrrolo-Cyt base (red) located at nucleotide Cyt75. **(d)** Fluorescence emission spectra for tRNApyr$^{Leu}$ (tRNA*) free or bound to different LeuRS$_{At}$ complexes.

**Table 1 | Isothermal titration calorimetry data showing binding of TM84 and/or tRNA$^{Leu}$ to LeuRS$_{At}$.**

| Complex | Model | $K_d$ (nM) | Stoichiometry | $\Delta H$ (kcal mol$^{-1}$) | $-T\Delta S$ (kcal mol$^{-1}$) | $\Delta G$ (kcal mol$^{-1}$) |
|---|---|---|---|---|---|---|
| LeuRS$_{At}$ · TM84 | One site | $152 \pm 20$ | $0.93 \pm 0.08$ | $-10.4 \pm 0.3$ | $0.95 \pm 0.4$ | $-9.4 \pm 0.08$ |
| LeuRS$_{At}$ · tRNA$^{Leu}$ · TM84 | Two site | $0.81 \pm 0.31$ | $0.51 \pm 0.03$ | $-18.8 \pm 0.9$ | $6.2 \pm 0.5$ | $-12.6 \pm 0.2$ |
| | | $14.4 \pm 1.37$ | $0.60 \pm 0.01$ | $-27.8 \pm 0.7$ | $16.3 \pm 0.5$ | $-10.8 \pm 0.01$ |
| LeuRS$_{At}$ · tRNA$^{Leu}$ | One site | $84.9 \pm 6.1$ | $0.93 \pm 0.01$ | $-16.2 \pm 0.6$ | $6.4 \pm 0.6$ | $-9.7 \pm 0.04$ |

two-site model with two TM84 binding sites with two different affinities of $0.81 \pm 0.31$ nM ($K_{d1}$) and $14.4 \pm 1.37$ nM ($K_{d2}$). Although a possible explanation for these results might be that the presence of tRNA creates a second TM84 binding site on the LeuRS$_{At}$ · tRNA complex, this is not possible as the total stoichiometry of binding in this case would be close to 2. Our data reveal stoichiometric values for the two binding events, $n1$ and $n2$, summing close to 1 ($n1 + n2 \approx 1$). Biphasic isotherms can be observed in heterotropic ligand-binding interactions to proteins that display co-operative ligand binding if one of the ligands is present at subsaturating concentration[30]. However, this possibility can be ruled out as the tRNA concentration

is saturating. Our results therefore suggest that, rather than observing two independent sites for TM84 on one protein, we are seeing the binding of TM84 to two distinct populations of LeuRS$_{At}$ · tRNA$^{Leu}$ with two different affinities for TM84.

A mixed population of LeuRS$_{At}$ · tRNA$^{Leu}$ complexes could originate in two ways. First, single-nucleotide resolution PAGE analysis of the transcript shows ∼11% of tRNAs with an additional nucleotide ($N+1$) added to the 3′-ends. This is a known side reaction of T7 RNA polymerase when catalysing *in vitro* transcription reactions[31]. Second, partially misfolded species, perhaps owing to lack of tRNA modifications, are also known to lead to lower percentages of tRNA transcripts that can

be aminoacylated. In our case, only ~50% of the tRNA$^{Leu}$ transcripts could be aminoacylated. Interestingly, binding of tRNA$^{Leu}$ to LeuRS$_{At}$ produces a monophasic isotherm, suggesting that the different tRNA$^{Leu}$ species have similar affinities for the enzyme that are indistinguishable from each other in the isotherm. However, the subsequent binding of TM84 can discriminate between the different LeuRS$_{At}$·tRNA$^{Leu}$ complexes, giving rise to biphasic isotherms reflecting different binding events.

A comparison of the isotherms indicates that TM84 is a relatively weak binder ($K_d = 152 \pm 20$ nM) to LeuRS$_{At}$ alone compared to binding to the enzyme pre-incubated with tRNA$^{Leu}$ ($K_d = 0.81 \pm 0.31$ nM high-affinity complex). The analysis indicates that binding of TM84 is enhanced up to ~200-fold in the presence of tRNA. If two different LeuRS$_{At}$·tRNA$^{Leu}$ complexes are considered, heterotropic interaction constants of 190 and 11 for each complex can be estimated from the ITC experiments[30], which correspond to cooperativity Gibbs energies of $-3.1$ and $-1.4$ kcal mol$^{-1}$, respectively. Therefore, tRNA$^{Leu}$ binding to LeuRS adds a 30% increase to the binding Gibbs energy for TM84. These findings are consistent with the results from our kinetics experiments that implicate tRNA$^{Leu}$ in the inhibition mechanism of TM84.

**TM84 binding to LeuRS·tRNA alters CCA 3′-end conformation.** The ITC results suggest that catalytically active tRNA and its CCA 3′-end may have an important role in facilitating the tight binding of TM84 in the ternary inhibition complex. To test this, we constructed a tRNA incorporating a fluorescent probe that is sensitive to the conformation and environment of the 3′-terminal nucleotides. We exchanged the penultimate Cyt75 residue of tRNA$^{Leu}$ with a fluorescent pyrrolo-cytidine nucleotide (Fig. 3c). This approach was used to monitor the conformation of the CCA 3′-end of tRNA$^{Cys}$ interacting with cysteinyl-tRNA synthetase[32]. By monitoring the fluorescence from this probe, we expected to see a significant change in the spectrum when the LeuRS·tRNApyr$^{Leu}$ complex was bound to TM84 or not. *E. coli* CCA nucleotidyl transferase was used to catalyse the addition of ATP and pyrCTP onto a truncated *in vitro* transcribed tRNA$^{Leu}$(UAA) sequence from *A. tumefaciens*. Importantly, the fluorescently labelled tRNApyr$^{Leu}$ was a substrate (if somewhat reduced in activity) for the aminoacylation reaction of LeuRS$_{At}$, indicating that the probe did not disrupt the interaction of the CCA 3′-end with the enzyme. We examined the fluorescence spectra of tRNApyr$^{Leu}$ alone, and in the presence of LeuRS$_{At}$ +/− TM84 or Leu-AMS. The emission fluorescence spectrum of tRNA$^{Leu}$ bound to LeuRS$_{At}$ shows a $\lambda_{max}$ of 456 nm (Fig. 3d). Addition of Leu-AMS to the protein–tRNA complex produces a fluorescence spectrum with similar intensity. However, addition of TM84 both increases the fluorescence intensity (~1.5-fold) and shifts the $\lambda_{max}$ by 5 nm. This unique TM84-induced spectral signal suggests that the toxin causes a rearrangement of the CCA 3′-end of the tRNA when bound to the LeuRS enzyme. Interestingly, this conformation of the CCA 3′-end of the tRNA does not appear to be substantially populated in the LeuRS·tRNApyr$^{Leu}$·Leu-AMS ternary complex.
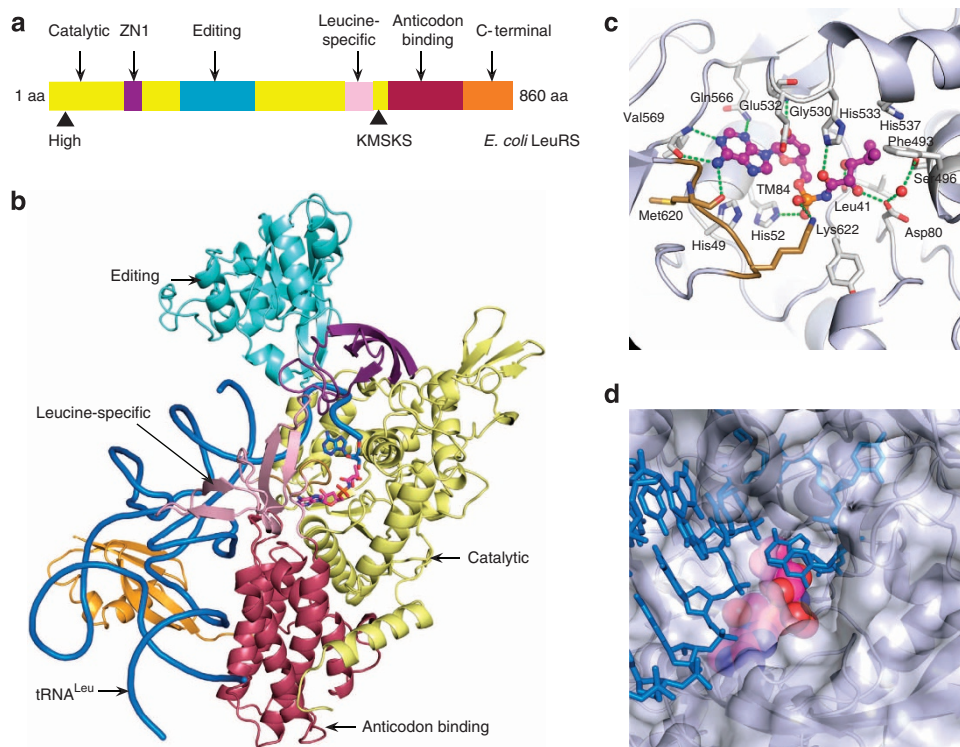
**Structure of the LeuRS·tRNA$^{Leu}$·TM84 inhibition complex.** To understand how TM84 binds to LeuRS and gain structural insights into the role of tRNA$^{Leu}$ in the unusual LeuRS inhibitory properties of TM84, we crystallized LeuRS in complex with tRNA$^{Leu}$ and TM84. We used recombinant *E. coli* LeuRS (LeuRS$_{Ec}$) and *in vitro* transcribed *E. coli* tRNA$^{Leu}$(UAA) iso-acceptor substrates, which have recently been shown to produce

high diffraction-quality crystals[21]. Importantly, LeuRS$_{Ec}$ shares 46% sequence identity with, and has similar domain architecture to, LeuRS$_{At}$ (Fig. 4a). LeuRS$_{Ec}$ has similar steady-state kinetic properties to that of LeuRS$_{At}$ (Supplementary Table S1) and aminoacylation by LeuRS$_{Ec}$ is potently inhibited by TM84 (Supplementary Fig. S3). The crystal structure of the LeuRS$_{Ec}$·tRNA$^{Leu}$·TM84 complex was solved by molecular replacement using the core of the complex formed by *Thermus thermophilus* LeuRS (LeuRS$_{Tt}$) with tRNA$^{Leu}$ [6], followed by building of the insertion domains. The model was refined to a final $R$-factor of 18.2% ($R$-free $= 23.6$%) at a final resolution of 2.4 Å (Fig. 4b; Table 2). The asymmetric unit contained two molecules of the ternary complex LeuRS·tRNA$^{Leu}$·TM84, one with slightly higher $B$-factors than the other.

The overall structure of the LeuRS$_{Ec}$·tRNA$^{Leu}$·TM84 complex (Fig. 4b) is very different from the previously described editing conformation of bacterial LeuRS[6]. Remarkably, it shows that the tRNA$^{Leu}$ acceptor stem is present in an 'aminoacylation-like' conformation, with the CCA 3′-end penetrating into the synthetic active site of LeuRS$_{Ec}$ where TM84 is bound (Fig. 4b,c; Supplementary Figs. S4, S5a). This suggests that TM84 causes inhibition of LeuRSs by resembling a stable form of Leu-AMP and thus prevents binding of the Leu and ATP substrates[16]. This finding also weakens an alternative hypothesis that proposes that the unusual inhibitory properties of TM84 are caused by the inhibitor binding to an alternative site on the enzyme other than the synthetic active site[8,33]. The most striking feature of the TM84 ternary structure is the pronounced movement of the highly conserved KMSKS loop across the active site of the enzyme when compared with previous LeuRS$_{Tt}$ structures bound to adenylate analogues[5,8] or tRNA[6] (Fig. 4d). The synthetic active site where TM84 is located is almost completely covered, encapsulating the ligand and presumably decreasing the dissociation rate of the inhibitor from the enzyme. The closed conformation of the KMSKS loop allows new protein–tRNA interactions that stabilize the aminoacylation conformation of the tRNA, notably the hydrogen bonds between the side chain of Lys619 and both the base of Cyt75 and phosphate of Gua71 (Supplementary Fig. S5a,b). Indeed, the structure shows that substantial re-ordering of the active site is mandatory for TM84 to form its 'aminoacylation-like' ternary complex. Interestingly, this is a property found in slow, tight-binding enzyme inhibitors[23].

To identify key interactions in the LeuRS ternary complex that may be responsible for the tRNA-dependence of TM84 binding, we made comparisons with a structure of LeuRS$_{Ec}$·tRNA$^{Leu}$·Leu-AMS captured in the functional aminoacylation conformation [21]. Leu-AMS, unlike TM84, does not show tRNA-dependent binding to LeuRS and as a consequence the tRNA could occupy more than one conformation on the enzyme in solution, an observation that is in accordance with our fluorescence data (Fig. 3d). Interestingly, the average B factors obtained from both structures do not reveal significant differences in the overall mobility of the two proteins in the crystal nor when individual B factors for domains are compared. A close comparison between the binding mode of TM84 (Fig. 4c) and Leu-AMS in their respective LeuRS$_{Ec}$·tRNA$^{Leu}$ 'aminoacylation-like' ternary complexes identifies a number of shared interactions between both ligands (His52, Phe493, Gly530, Glu532, His533, His537, Gln566, Val569 and Met620), but also reveals key variations between the binding mode exhibited by the two ligands (Fig. 5a–c) that could explain their fundamental difference in tRNA-dependency. The chemical structures of TM84 and Leu-AMS are different, which is reflected in the differential binding and inhibition behaviours exhibited by the two molecules. In TM84, the Leu side-chain is replaced by a substituted methyl pentanamide with an OH group (C2-OH) replacing the α-amino

**Figure 4 | Structure of the LeuRS$_{Ec}$·tRNA$^{Leu}$·TM84 inhibition complex.** (**a**) Domain structure of LeuRS$_{Ec}$. (**b**) Structure of LeuRS$_{Ec}$·tRNA$^{Leu}$·TM84 complex in 'aminoacylation-like' conformation. Domains coloured and labelled, tRNA$^{Leu}$ (blue) with Ade76 and TM84 depicted with stick bonds in synthetic active site. (**c**) Active site interactions with TM84. (**d**) Encapsulation of TM84 (space filling model—pink) in synthetic active site. LeuRS$_{Ec}$ protein surface—grey and tRNA$^{Leu}$—blue.

group and an additional OH group on the side-chain (C3-OH) (Fig. 1b). The C2-OH of the methyl pentanamide group of TM84 forms a hydrogen bond with Asp80, mimicking the interaction with the α-amino group as in the Leu-AMS bound protein. However, the main chain carbonyl oxygen of Leu41 hydrogen bonds to the C3-OH of TM84 (Fig. 5a), whereas in the Leu-AMS complex, it only hydrogen bonds with the α-amino group (Fig. 5b). TM84 also contains a 3-deoxyarabinose sugar ring substituting for the ribose found in Leu-AMP/Leu-AMS. In the Leu-AMS-bound structure, the ribose 2′-OH and 3′-OH groups, each make a hydrogen bond with active site residue Gly530 (Fig. 5b). However, the loss of the *cis*-diol from the TM84 sugar results in only a single hydrogen bond between its 2′-OH group and Gly530 that extends above the plane of the sugar ring (Fig. 5a). Perhaps the most striking and intriguing difference between the two ternary complexes is in the ribose pucker of the terminal adenosine (Ade76). In the Leu-AMS functional aminoacylation state, this ribose is in a C2′-*exo* conformation, allowing the 2′-OH to point towards the carbonyl-carbon of Leu-AMS (Fig. 5b,c) as would be expected prior to the transfer step in the aminoacylation reaction[21]. In the TM84 complex, the Ade76 ribose is in an unexpected C2′-*endo* conformation, resulting in the 2′-OH pointing away from the carbonyl-carbon and instead forming a hydrogen bond to a nearby water molecule that in turn hydrogen bonds to Asp80 and Ser496 (Fig. 5a,c). The altered position of the 3′-OH allows it to make a direct hydrogen bond to the C2-OH of TM84. This direct interaction between tRNA$^{Leu}$ and TM84 may play an additional role in stabilizing the ternary inhibition complex.

Importantly, there is also a significant difference between the KMSKS loop conformation for the two ligands. Whereas in the Leu-AMS ternary complex the second Lys of the K[619]MSK[622]S loop (Lys622) points away from the active site (Fig. 5b), in the TM84 complex Lys622 points right into the active site and interacts with a non-bridging oxygen of the negatively charged N-acyl phosphate group of TM84 (Fig. 5a; Supplementary Fig. S5b). The positioning of Lys622 is also a contributing factor in the reduced solvent accessibility of TM84 when bound to the LeuRS$_{Ec}$ (20.6 Å$^2$) compared to Leu-AMS (44.2 Å$^2$). Several factors may contribute to the different conformations exhibited by Lys622 in the two structures. First, the insertion of positively charged Lys622 into the active site is electrostatically favoured both by the presence of the charged N-acyl phosphate group and by the absence of the α-amino group in the case of TM84. In contrast, for Leu-AMS, the sulphate is uncharged. Second, the particular C2′-*endo* ribose pucker of Ade76 in the TM84 complex avoids potential steric hindrance of Lys622 entering the site, which would be the case with the functional C2′-*exo* conformation. Interestingly, His52, the second histidine residue of the H[49]IGH[52] catalytic motif, makes an interaction with the other non-bridging oxygen of the phosphate moiety of TM84 (Fig. 4c). Although the ionic interaction between Lys622 and the α-phosphate of TM84 is not seen in other LeuRS structures bound to the adenylate analogue (but it remains to be seen what would happen with the true negatively charged Leu-AMP), an equivalent interaction was found in a GlnRS·tRNA$^{Gln}$·Gln-AMS 'aminoacylation' structure[10]. However, the conformation of the KMSKS loop in this structure does not close so fully over the synthetic active site as in the LeuRS ternary complexes. The observed position of the second lysine of the KMSKS catalytic peptide in the TM84 complex more resembles the conformation expected for the amino-acid activation reaction, as this residue is known to have an important role in both catalysis of activation and the binding of the α and γ phosphates of ATP[34].
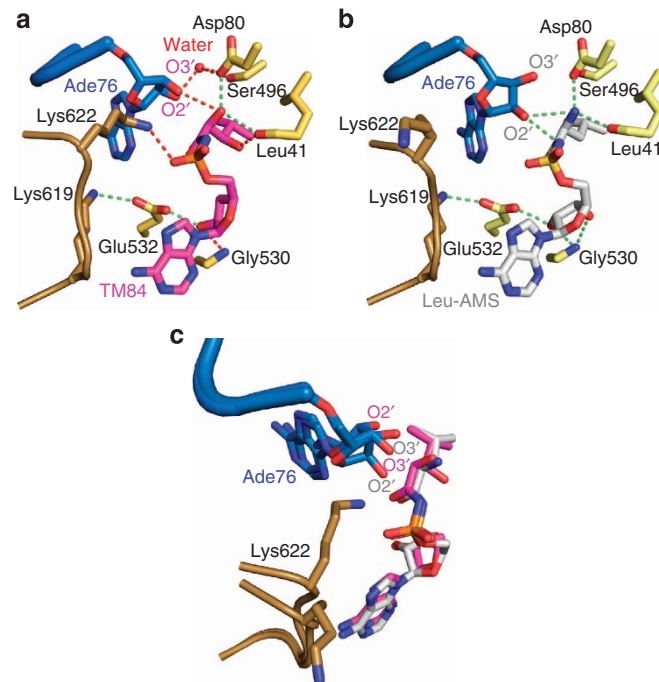
**Table 2 | Data collection and refinement statistics.**

| Data collection | E. coli LeuRS + E. coli tRNALeu(UAA) + TM84 |
|---|---|
| Space group | C2 |
| *Cell dimensions* | |
| a, b, c (Å) | 158.58, 68.19, 226.22 |
| α, β, γ (°) | 90°, 105.53°, 90° |
| Solvent content (%) | 53.5 |
| Beamline | ESRF ID14-4 |
| Wavelength (Å) | 0.9395 |
| Detector | ADSC quantum Q315r |
| Resolution range of data (last shell) (Å) | 43.59–2.4 (2.40–2.50) |
| Completeness (last shell) (%) | 93.3 (65.1) |
| R-sym (last shell) | 0.104 (0.435) |
| I/σI (last shell) | 10.2 (1.8) |
| Redundancy (last shell) | 3.91 (1.7) |
| *Refinement* | |
| No. of reflections used in refinement work (free) | 80,975 (4,280) |
| R-factor (last shell) | 0.187 (0.343) |
| R-free (last shell) | 0.238 (0.389) |
| No.of non-H atoms: total | 17,522 |
| Protein | 13,717 |
| tRNA | 3,367 |
| Ligand | 62 |
| Solvent | 369 water, 7 Mg$^{2+}$ |
| Mean B-value (Å$^2$) | 48.8 |
| *Quality* | |
| Ramachandran plot (%) | |
| Favoured regions | 96.7 |
| Allowed regions | 99.8 |
| Disallowed regions | 0.2 (4 outliers/1,716 residues) |
| R.m.s. deviations | |
| Bond distances (Å) | 0.010 |
| Bond angles (°) | 1.45 |



**Figure 5 | Comparison of TM84 and Leu-AMS bound in LeuRS$_{Ec}$ ternary complexes.** (**a**) TM84 (pink) binding in the synthetic active site showing interactions with the KMSKS loop (gold) and the terminal tRNA Ade76 (blue). The ribose of the adenosine is in the C2′-*endo* conformation. Water molecule depicted as a red sphere. (**b**) Leu-AMS (grey) in its respective ternary complex. The ribose of the adenosine in this structure is in the C2′-*exo* conformation. (**c**) Superimposition of the two ligands in their respective ternary complexes.

## Discussion

Our biophysical and biochemical analyses elucidate a new tRNA-dependent LeuRS inhibition mechanism for TM84, which clearly distinguishes it from Leu-AMS. The crystal structure of the TM84 ternary complex, however, only reveals subtle differences. The binding of TM84 to the LeuRS$_{At}$ active site in the absence of tRNA is considerably weaker than that observed for Leu-AMS. A number of interactions found in Leu-AMS-bound structures[5,21] that are absent when TM84 is bound (Figs. 4c, 5a,b) may explain the reduced affinity of TM84 for LeuRS$_{At}$ in the absence of tRNA. These include loss of hydrogen bonds to the sugar moiety of the nucleotide and loss of a potential ionic interaction with Leu-AMS when its amino group is replaced with a hydroxyl in TM84. The crystal structure also reveals three additional interactions that are formed in the presence of tRNA: Lys619 to Cyt75; Lys622 to the phosphate of TM84; and Ade76 to TM84 (Supplementary Fig. S5b). We hypothesize that absence of tRNA and concomitant loss of two of these interactions lead to increased KMSKS loop mobility, and destabilization of the Lys622 interaction with TM84.

The role of tRNA and the KMSKS loop in binding TM84 also raises kinetic questions about the exact order of binding events. TM84 has to bind to an open active site prior to the positioning of the CCA 3′-end in the final closed ternary complex, leading to decreased dissociation of TM84 (slow $k_{off}$ rate). What is not clear,

is how rapidly TM84 binds to the open active site ($k_{on}$); how tRNA might affect this initial binding event; or whether the KMSKS loop binds to TM84 independently of the CCA 3′-end or not. Pre-steady-state kinetic analysis is required to determine the precise order of these events.

Why would nature evolve a Trojan Horse LeuRS inhibitor[16] with a tRNA-dependent inhibition mechanism? Perhaps when LeuRS$_{At}$ is inhibited, substrate concentrations would be expected to rise in agrobacterial cells. Under these conditions, a simple LeuRS competitive inhibitor might have decreased toxicity, whereas the higher concentrations of deacylated tRNA$^{Leu}$ would increase the affinity of TM84 for the enzyme. Whatever the reason, this study provides insight into a novel tRNA-dependent inhibitor of LeuRS with potential ramifications for rational antibiotic design.

## Methods

**Protein expression and purification.** LeuRS$_{At}$ was expressed in *E. coli* BL21 (DE3) RIL codon plus cells containing the pET-21b plasmid encoding LeuRS$_{At}$ with a carboxy-terminal 6X-histidine tag (the *leuS*$_{At}$ gene had been subcloned in to pET-21b using *Nde*I and *Xho*I restriction sites)[16]. Cells were grown in Luria broth at 37 °C, with appropriate antibiotics, to an optical density of 0.3–0.4 (measured at $A_{600}$) before induction with 1 mM isopropyl-B-D-thiogalactopyranoside. The cells were grown for an additional 3–4 h at 24 °C before harvesting by centrifugation at 5,400 *g* for 10 min. Cells were lysed by sonication in standard Qiagen lysis buffer. The soluble His-tagged LeuRS$_{At}$ protein was purified using Ni-NTA agarose (Qiagen) as detailed by the manufacturer. The protein was further purified by FPLC using a Mono-Q column and a gradient of 20 mM NaCl to 500 mM NaCl in Tris–HCl buffer (pH 8.0). The purified protein was confirmed to be >95% pure using SDS–polyacrylamide gel electrophoresis. Active LeuRS$_{At}$ protein concentration for kinetic assays was determined by active site titration (see below).

LeuRS$_{Ec}$ used for structural studies was expressed in *E. coli* BL21 cells containing pET-15b plasmid encoding LeuRS$_{Ec}$ with an amino-terminal 6X-histidine tag (MGSSHHHHHHSSGLVPRGSH) under similar conditions[21].

**TM84 purification**. Agrocin 84 (purified as detailed previously[16]) was incubated in sodium phosphate buffer (pH 7.0) at 100 °C for 15 min and the liberated TM84 toxin was separated from other reaction products by reverse-phase high-performance liquid chromatography. The concentration of purified TM84 was determined using an extinction coefficient ($\varepsilon_{260\,nm}$) of 0.0154 $M^{-1}\,cm^{-1}$.

**tRNA^Leu transcription**. Plasmids encoding tRNA$^{Leu}$(UAA) isoacceptor sequences from *A. tumefaciens* C58 or *E. coli* in front of T7 polymerase promoter sequences were purified from *E. coli* DH5-α cells before digestion overnight at 60 °C with *Bst*NI restriction enzyme to linearize the plasmid DNA. The transcription reaction was performed using template DNA (450 μg), 9 μM T7 RNA polymerase[35], 1 U ml$^{-1}$ RNAse inhibitor, 40 mM Tris-HCl (pH 8.0), 25 mM MgCl$_2$, 40 mM DTT, 0.1% Triton X-100, 1 mM spermidine and 2 mM rNTPs. The reaction mix was incubated at 37 °C overnight before quenching with 50 mM EDTA followed by *DNase I* digestion for 1 h to remove template DNA. Phenol–chloroform extraction (pH 5.2) followed by ethanol precipitation (using 0.3 M sodium acetate) isolated the tRNA from the reaction. The precipitated tRNA was gel purified on a 12% denaturing polyacrylamide gel electrophoresis (19:1), 8 M urea gel and 1 × Tris-borate EDTA buffer (pH 8.3). After gel extraction, elution and ethanol precipitation, the purified tRNA$^{Leu}$(UAA) was refolded by denaturing at 95 °C for 1 min, followed by addition of 1 mM MgCl$_2$, and gradually cooled to 28 °C for 1 h. The concentration of refolded tRNA$^{Leu}$ was determined using a theoretical extinction coefficient ($\varepsilon_{260}$) of 531,500 $M^{-1}\,cm^{-1}$ modified by a factor of 1.34 to account for the hypochromic effect of tRNA folding on absorbance.

**Active site titration assay**. The concentration of active LeuRS enzyme for kinetic assays was determined by active site titration as described previously[25]. The reaction buffer contained 50 mM HEPES buffer (pH 7.4), 20 mM KCl, 10 mM MgCl$_2$, 10 mM β-mercaptoethanol (β-ME), 1 mM L-Leu, 5 μg/ml inorganic pyrophophatase, 5 μM ATP, 4 μCi [γ-$^{32}$P] ATP and purified recombinant LeuRS enzymes ranging in total protein concentration from 1 to 2 μM (determined by Biorad Protein assay). The reaction was carried out at 28 °C and 5 μl time point aliquots collected. The assay was performed in triplicate and the active enzyme concentration was determined by measuring the amplitude of the burst phase of Leu-AMP formation[24,25].

**ATP/PPi exchange assay**. The ATP/PPi exchange assays were performed as detailed earlier[25]. Reaction mixtures containing 50 mM HEPES buffer (pH 7.4), 20 mM KCl, 10 mM MgCl$_2$, 500 μM L-Leu, 4 mM ATP, 1 mM tetrasodium pyrophosphate (NaPPi), 10 μCi mmol$^{-1}$ [$^{32}$P] NaPPi, 1 μM bovine serum albumin and LeuRS$_{At}$ (1–2 nM) were incubated at 28 °C. LeuRS$_{At}$ enzyme was pre-incubated for 1 h with inhibitor $+/-$ tRNA$^{Leu}$ (6.7 μM) in appropriate experiments and the reactions were initiated by addition of 4 mM ATP and incubated at 28 °C (LeuRS$_{At}$) or 37 °C (LeuRS$_{Ec}$). Five-microlitre aliquots for each time point were collected, acid quenched and processed[25]. The amount of [$^{32}$P]-PPi incorporation into ATP was measured by liquid scintillation counting.

**Aminoacylation assay**. The 40-μl leucylation reaction mixtures contained 50 mM HEPES (pH 7.4), 20 mM KCl, 25 mM MgCl$_2$, 25 mM β-ME, 4 mM ATP, 500 μM [3,4,5-$^3$H] L-Leu (20 μCi mmol$^{-1}$), 5 μg/ml inorganic pyrophosphatase and 13.4 μM of active *in vitro* transcribed tRNA$^{Leu}$ (50% tRNA$^{Leu}$(UAA) is active based on tRNA charging at saturating enzyme and substrate concentrations). Reactions were initiated with 1–8 nM of active LeuRS enzyme that had been pre-incubated for 1 h with the tRNA$^{Leu}$ substrate $+/-$ inhibitor. Reactions were incubated at 28 °C (LeuRS$_{At}$) or 37 °C (LeuRS$_{Ec}$). Five-microlitre aliquots of the reaction mix were spotted on 5% trichloroacetic acid (TCA) pre-soaked filter pads, washed twice with 5% TCA and then with 70% ethanol at 4 °C. The pads were dried and quantified using scintillation counting. Initial rates (within the first 10–15% part of the reaction) were obtained and an average rate from three individual data sets was used to plot the dose–response curve, which was fit to a standard form of the Morrison equation for tight-binding inhibitors (see below).

Morrison equation:

$$\frac{v_i}{v_0} = 1 - \frac{([E] + [I] + K_i^{app}) - \sqrt{([E] + [I] + K_i^{app})^2 - 4[E][I]}}{2[E]} \quad (1)$$

**Steady-state fluorescence**. The penultimate base of the appropriate tRNA-$^{Leu}$(UAA) isoacceptor was labelled with a pyrrolo-cytidine fluorophore. To achieve labelling, *E. coli* tRNA nucleotidyl transferase enzyme was incubated with a truncated in vitro tRNA transcript and pyrrolo-CTP (Trilink Biotechnologies) and ATP as outlined previously[32]. Fluorescence experiments were performed in buffer containing 50 mM HEPES (pH 7.4), 20 mM KCl, 10 mM MgCl$_2$ and 10 mM β-ME at 28 °C. Briefly, 0.2 μM pyrrolo-C labelled fluorescent tRNA$^{Leu}$(UAA) isoacceptor was added to 1 μM LeuRS$_{At}$ and 2.5 μM TM84 or Leu-AMS. The fluorescence spectra were collected on a Horiba Fluoromax-2 fluorimeter. The excitation wavelength was 352 nm and emission was measured between 390–600 nm. Excitation and emission slit widths were both 5 nm. The spectra were analysed with Datamax software and corrected with appropriate blanks to obtain the final spectra.

**Isothermal titration calorimetry**. TM84 interactions with LeuRS$_{At}$ were explored using a VP-ITC and an Auto-ITC200 microcalorimeter (MicroCal/GE Healthcare). All solutions were prepared in buffer containing 50 mM HEPES (pH 7.4), 20 mM KCl, 10 mM MgCl$_2$ and 1 mM β-ME. For thermodynamic experiments, LeuRS$_{At}$ active protein concentration was determined using ITC titration of a tight-binding ligand (Leu-AMS) to LeuRS$_{At}$ as detailed elsewhere[36]. LeuRS$_{At}$ (active protein concentrations ranging from 4 to 8 μM) was placed in the sample cell and the ligand (at a concentration 10-fold higher than that of the protein) was placed in the syringe. In the ternary titrations, tRNA$^{Leu}$ was added to LeuRS in the cell at a 1:1.2 molar ratio. Titrations were carried out at pH 7.4 and 28 °C. The injection volume was 5–15 μl and the time between injections was 180–240 s. The data were analysed using Origin for ITC software (version 7), and fitted to a one-site or a two-site binding model (due to mixing artefacts, the heat associated with the first peak was excluded from the data analysis). Binding affinity ($K_d$), stoichiometry ($N$) and enthalpy ($\Delta H$) for each complex were determined. The c-values ($= [P_{total}] \times K_a$) in our experiments varied from 4 to 900, well within the suggested range of 1–1,000 (ref. 37).

**Crystallization and X-ray data collection**. To crystallize the LeuRS$_{Ec}$ · tRNA$^{Leu}$ · TM84 complex, a 2-μl aliquot of the solution containing the complex was mixed with 2 μl of a crystallization solution and then equilibrated by hanging-drop vapour diffusion against 500 μl of reservoir solution. Crystals appeared at 273 K within 4–5 days in 0.1 M Bis-TRIS at pH 5.5 and 23–25% PEG 3350.

For data collection, crystals were flash-cooled directly in liquid nitrogen. Diffraction data were collected at 100 K at the European Synchrotron Radiation Facility on beamline ID14-EH4 (ESRF, Grenoble, France). Crystals were of space-group C2 with two molecules of complex per asymmetric unit. Data sets were integrated and scaled using the XDS suite[38]. Subsequent data analysis was performed with the CCP4 suite.

**Structure determination and refinement**. The structure was solved by molecular replacement (PHASER[39]) using the core of the protein from the LeuRS$_{Ec}$ editing complex (1–223, 416–568 and 795–860 residues[21]). The resulting model was used to search for the core of the tRNA (bases 5–79) and to manually build the external flexible domains using COOT[40]. The Zn domain (158–189), not visible in the LeuRS$_{Ec}$ editing complex, was built using the analogous *T. thermophilus* LeuRS structure as a guide. Models were refined by rigid-body refinement, followed by isotropic *B*-factor refinement using REFMAC5 with translation libration screw-motion[41]. In the resultant $2m|F_o| - D|F_c|$ and $m|F_o| - D|F_c|$ maps, we clearly found both tRNA and TM84 electron densities. The crystallographic data collection and final refinement statistics are presented in Table 1. Several hydrated magnesium ions are observed within the tRNAs.

## References

1. Soll, D. & Schimmel, P. R. *Aminoacyl-tRNA Synthetases* 3rd edn, Vol. 10. (Academic Press, 1974).
2. First, E. A. & Fersht, A. R. Analysis of the role of the KMSKS loop in the catalytic mechanism of the tyrosyl-tRNA synthetase using multimutant cycles. *Biochemistry* **34**, 5030–5043 (1995).
3. Ibba, M. & Soll, D. Aminoacyl-tRNA synthesis. *Annu. Rev. Biochem.* **69**, 617–650 (2000).
4. Hsu, J. L., Rho, S. B., Vannella, K. M. & Martinis, S. A. Functional divergence of a unique C-terminal domain of leucyl-tRNA synthetase to accommodate splicing and aminoacylation roles. *J. Biol. Chem.* **281**, 23075–23082 (2006).
5. Cusack, S., Yaremchuk, A. & Tukalo, M. The 2 A crystal structure of leucyl-tRNA synthetase and its complex with a leucyl-adenylate analogue. *EMBO J.* **19**, 2351–2361 (2000).
6. Tukalo, M., Yaremchuk, A., Fukunaga, R., Yokoyama, S. & Cusack, S. The crystal structure of leucyl-tRNA synthetase complexed with tRNALeu in the post-transfer-editing conformation. *Nat. Struct. Mol. Biol.* **12**, 923–930 (2005).
7. Fukunaga, R. & Yokoyama, S. Aminoacylation complex structures of leucyl-tRNA synthetase and tRNALeu reveal two modes of discriminator-base recognition. *Nat. Struct. Mol. Biol.* **12**, 915–922 (2005).
8. Lincecum, Jr. T. L. *et al.* Structural and mechanistic basis of pre- and posttransfer editing by leucyl-tRNA synthetase. *Mol. Cell* **11**, 951–963 (2003).
9. Schimmel, P., Tao, J. & Hill, J. Aminoacyl tRNA synthetases as targets for new anti-infectives. *FASEB J.* **12**, 1599–1609 (1998).
10. Rath, V. L., Silvian, L. F., Beijer, B., Sproat, B. S. & Steitz, T. A. How glutaminyl-tRNA synthetase selects glutamine. *Structure* **6**, 439–449 (1998).
11. Berthet-Colominas, C. *et al.* The crystal structure of asparaginyl-tRNA synthetase from Thermus thermophilus and its complexes with ATP and asparaginyl-adenylate: the mechanism of discrimination between asparagine and aspartic acid. *EMBO J.* **17**, 2947–2960 (1998).
12. Silvian, L. F., Wang, J. & Steitz, T. A. Insights into editing from an ile-tRNA synthetase structure with tRNAile and mupirocin. *Science* **285**, 1074–1077 (1999).
13. Pope, A. J. *et al.* Characterization of isoleucyl-tRNA synthetase from *Staphylococcus aureus*. II. Mechanism of inhibition by reaction intermediate

and pseudomonic acid analogues studied using transient and steady-state kinetics. *J. Biol. Chem.* **273,** 31691–31701 (1998).

14. Forrest, A. K. *et al.* Aminoalkyl adenylate and aminoacyl sulfamate intermediate analogues differing greatly in affinity for their cognate *Staphylococcus aureus* aminoacyl tRNA synthetases. *Bioorg. Med. Chem. Lett.* **10,** 1871–1874 (2000).

15. Tate, M. E., Murphy, P. J., Roberts, W. P. & Kerr, A. Adenine N6-substituent of agrocin 84 determines its bacteriocin-like specificity. *Nature* **280,** 697–699 (1979).

16. Reader, J. S. *et al.* Major biocontrol of plant tumors targets tRNA synthetase. *Science* **309,** 1533 (2005).

17. Kerr, A. & Tate, M. in *Agrobacterium Tumefaciens: From Plant Pathology to Biotechnology* (eds Nester, E., Gordon, M. P. & Kerr, A.) (APS Press, 2004).

18. Chilton, M. D. *et al.* Stable incorporation of plasmid DNA into higher plant cells: the molecular basis of crown gall tumorigenesis. *Cell* **11,** 263–271 (1977).

19. Murphy, P. J., Tate, M. E. & Kerr, A. Substituents at N6 and C-5′ control selective uptake and toxicity of the adenine-nucleotide bacteriocin, agrocin 84, in Agrobacteria. *Eur. J. Biochem.* **115,** 539–543 (1981).

20. Ryder, M. H., Tate, M. E. & Jones, G. P. Agrocinopine A, a tumor-inducing plasmid-coded enzyme product, is a phosphodiester of sucrose and L-arabinose. *J. Biol. Chem.* **259,** 9704–9710 (1984).

21. Palencia, A. *et al.* Structural dynamics of the aminoacylation and proofreading functional cycle of bacterial leucyl-tRNA synthetase. *Nat. Struct. Mol. Biol.* **19,** 677–6847 (2012).

22. Copeland, R. A. *Enzymes: A Practical Introduction to Structure, Mechanism and Data Analysis.* 2nd edn (Wiley-VCH (2000).

23. Morrison, J. F. & Walsh, C. T. The behavior and significance of slow-binding enzyme inhibitors. *Adv. Enzymol. Relat. Areas. Mol. Biol.* **61,** 201–301 (1988).

24. Francklyn, C. S., First, E. A., Perona, J. J. & Hou, Y. M. Methods for kinetic and thermodynamic analysis of aminoacyl-tRNA synthetases. *Methods* **44,** 100–118 (2008).

25. Beebe, K., Waas, W., Druzina, Z., Guo, M. & Schimmel, P. A universal plate format for increased throughput of assays that monitor multiple aminoacyl transfer RNA synthetase activities. *Anal. Biochem.* **368,** 111–121 (2007).

26. Freist, W., Gauss, D. H., Ibba, M. & Soll, D. Glutaminyl-tRNA synthetase. *Biol. Chem.* **378,** 1103–1117 (1997).

27. Freist, W., Gauss, D. H., Soll, D. & Lapointe, J. Glutamyl-tRNA sythetase. *Biol. Chem.* **378,** 1313–1329 (1997).

28. Neubig, R. R., Spedding, M., Kenakin, T. & Christopoulos, A. International Union of Pharmacology Committee on Receptor Nomenclature and Drug Classification. XXXVIII. Update on terms and symbols in quantitative pharmacology. *Pharmacol. Rev.* **55,** 597–606 (2003).

29. Poulin, R., Lu, L., Ackermann, B., Bey, P. & Pegg, A. E. Mechanism of the irreversible inactivation of mouse ornithine decarboxylase by alpha-difluoromethylornithine. Characterization of sequences at the inhibitor and coenzyme binding sites. *J. Biol. Chem.* **267,** 150–158 (1992).

30. Velazquez-Campoy, A., Goni, G., Peregrina, J. R. & Medina, M. Exact analysis of heterotropic interactions in proteins: characterization of cooperative ligand binding by isothermal titration calorimetry. *Biophys. J.* **91,** 1887–1904 (2006).

31. Sherlin, L. D. *et al.* Chemical and enzymatic synthesis of tRNAs for high-throughput crystallization. *RNA* **7,** 1671–1678 (2001).

32. Zhang, C. M. *et al.* Pyrrolo-C as a molecular probe for monitoring conformations of the tRNA 3′ end. *RNA* **14,** 2245–2253 (2008).

33. Rock, F. L. *et al.* An antifungal agent inhibits an aminoacyl-tRNA synthetase by trapping tRNA in the editing site. *Science* **316,** 1759–1761 (2007).

34. Perona, J. J., Rould, M. A. & Steitz, T. A. Structural basis for transfer RNA aminoacylation by *Escherichia coli* glutaminyl-tRNA synthetase. *Biochemistry* **32,** 8758–8771 (1993).

35. He, B. *et al.* Rapid mutagenesis and purification of phage RNA polymerases. *Protein Expr. Purif.* **9,** 142–151 (1997).

36. Schön, A. & Velazquez-Campoy, A. in *Methods for Structural Analysis of Protein Pharmaceuticals.* Chapter 17, 573–589 (AAPS Press, 2005).

37. Wiseman, T., Williston, S., Brandts, J. F. & Lin, L. N. Rapid measurement of binding constants and heats of binding using a new titration calorimeter. *Anal. Biochem.* **179,** 131–137 (1989).

38. Kabsch, W. Xds. *Acta. Crystallogr. D* **66,** 125–132 (2010).

39. McCoy, A. J. *et al.* Phaser crystallographic software. *J. Appl. Crystallogr.* **40,** 658–674 (2007).

40. Emsley, P., Lohkamp, B., Scott, W. G. & Cowtan, K. Features and development of coot. *Acta Crystallogr. D* **66,** 486–501 (2010).

41. Murshudov, G. N., Vagin, A. A. & Dodson, E. J. Refinement of macromolecular structures by the maximum-likelihood method. *Acta. Crystallogr. D* **53,** 240–255 (1997).

## Acknowledgements

## Author contributions

J.S.R. and S.Ch. performed project design and interpretation. S.Ch. conducted biochemical and biophysical experiments, data analyses and contributed to manuscript writing. A.P. and S.Cu. performed X-ray crystallography and solved the structure of the LeuRS$_{Ec}$·tRNA·TM84 complex. C.V. purified TM84. A.T. and A.V.C. provided expertise on ITC data analyses. B.T. assisted in interpretation of structural data and in producing the figures. J.S.R. prepared the manuscript. All authors read and assisted in editing the manuscript.

## Additional information

**Accession codes:** Atomic coordinates and structure factors for the LeuRS$_{Ec}$·tRNA·TM84 ternary complex have been deposited in the RCSB Protein Data Bank under accession code 3zgz.

**Supplementary Information** accompanies this paper at http://www.nature.com/naturecommunications

**Competing financial interests:** The authors declare no competing financial interests.

**Reprints and permission** information is available online at http://npg.nature.com/reprintsandpermissions/

**How to cite this article:** Chopra, S. *et al.* Plant tumour biocontrol agent employs a tRNA-dependent mechanism to inhibit leucyl-tRNA synthetase. *Nat. Commun.* 4:1417 doi: 10.1038/ncomms2421 (2013).